Supporting Information

Fast Lithium Ion Transport Pathways Constructed by Two-Dimensional Boron Nitride Nanoflakes in Quasi-Solid-State Polymer Electrolyte

Jinghan Zuo, [1,⊥] Yan Dang,[1,⊥] Pengbo Zhai,[2] Bixuan Li,[3] Lei Wang,[1] Moxuan Wang,[1] Zhilin Yang,[3] Qian Chen,[1] Xiaokang Gu,[1] Zeyang Li,[4] Peizhe Tang*[,1,5] and Yongji Gong*[,1,2]

[1]*School of Materials Science and Engineering, Beihang University, Beijing 100191, China*

[2]*Tianmushan Laboratory, Xixi Octagon City, Hangzhou 310023, China*

[3]*School of Physics, Beihang University, Beijing 100191, China*

[4]*School of Computer Science, Fudan University, Shanghai 200438, China*

[5]*Center for Free-Electron Laser Science, Max Planck Institute for the Structure and Dynamics of Matter, Hamburg 22761, Germany*

Author Contributions

[⊥]J.Z. and Y.D. contributed equally.

Corresponding Author

*E-mail: *peizhet@buaa.edu.cn*

*E-mail: *yongjigong@buaa.edu.cn*

Experimental Section

Materials

The following materials are used in this study: lithium difluoro(oxalate)borate (LiDFOB, 99.9%), lithium perchlorate ($LiClO_4$, 99.9%), monomer vinylene carbonate liquid (VCA, 98%), 1,4-Naphthoquinone (98%) and 2,2'-Azobis(2-methyl propionitrile) (AIBN, 98%) was purchased from Innochem (Beijing) Technology Co., Ltd. Boron nitride nanoflakes (BNNFs, 99%) was purchased from Zhongruitai Technology Co., Ltd. All the materials were used without further purification.

Quasi-solid-state electrolyte synthesis.

The PVCA-BNNF QSSE is fabricated via the following process. Firstly, 1.43 g LiDFOB or 1.06 g $LiClO_4$ was dissolved in 10 mL VCA to get a homogeneous and transparent solution (1.0 M LiDFOB or $LiClO_4$ in VCA). Then 6.1 mg ml^{-1} BNNF was added to the solution followed by 8-hour ultrasonic dispersion, and 2.2 mg ml^{-1} AIBN, was added to obtain the polymerization precursor. In this work, the as-prepared precursor was poured into a 50×50 mm^2 poly(tetrafluoroethylene) mold with different depths and kept constantly at 60 ℃ for 14 h in a hot box. After the mold cooled to room temperature, the electrolyte was removed from the mold and cut into desired size and shape. Next, it was immersed in a polarization termination solution (3 mg ml^{-1}, 1,4-Naphthoquinone in VCA) for 1 min and the residual solution was gently wiped off. It was then placed in an Ar-filled glovebox until its weight reached steady before the PVCA-BNNF QSSE was obtained.

The PVCA QSSE was fabricated likewise, only without the addition of the BNNFs.

Material characterization.

The BNNFs and QSSEs were studied using a scanning electron microscope (SEM, Hitachi SU8020) and a transmission electron microscope (TEM, JEOLJEM 2100F). The nanoparticle sizes of BNNFs dispersed in VCA (6.1 mg mL^{-1}) were measured using Zetasizer Nano ZS ZEN3600 (Malvern Instruments Ltd., England). A nitrogen

adsorption-desorption surface area analyzer was used to calculate the specific surface area (ASAP 2460, Micromeritics Co., USA). At a tensile stretch rate of 10 mm min^{-1}, the mechanical properties of the samples were investigated using an electronic universal material testing machine (Zwick/Roell Z0.5, Zwick/Roell Testing Technology (Shanghai) Co., Ltd). Raman spectra were analyzed at 532 nm using a HORIBA LabRAM HR Evolution system. The IR spectra of the samples were recorded using Fourier transform infrared spectroscopy (FT-IR, Nicolet IS 50) in the 400–4000 cm^{-1} range. The TOF-SIMS 5 IONTOF (Münster, Germany) was used for the Time-of-Flight Secondary Ion Mass Spectrometry (TOF-SIMS). In the test, we adopted an h-BN film, which is synthesized using the standard chemical vapor deposition (CVD) method[1, 2], to simulate the BNNF used in the PVCA-BNNF QSSE. To simulate the solvent environment around the BNNF, one drop of VCA solution (1M LiDFOB) is spin-casted on the h-BN film. When compared to in-situ characterizing the BNNFs in PVCA-BNNF QSSE, such simulation can avoid the difficulty of in-situ locating the BNNFs in the electrolyte and eliminate the error caused by the tilt orientation of BNNFs. To ensure the universality and accuracy of the test results, the central part (135 × 135 μm^2) of a large sputter area (300 × 300 μm^2) is investigated in the test for the depth profiles. ^{7}Li NMR of VCA and VCA-BNNF (1M LiDFOB) was carried out using Avance NEO 600 NMR spectrometer (600 MHz/Bruker, Germany).

Battery assembly

All batteries were assembled with CR2032 coin-type cells in an argon-filled glovebox (H_2O < 0.1 ppm, O_2 < 0.1 ppm). The Li/Li symmetric cells were assembled with electrolytes sandwiched between two Li electrodes (diameter: 15.6 mm, thickness: 0.45mm). Li plating /stripping behavior was evaluated on the NEWARE battery testing system at 25 °C. The commercial LFP and NCM811 cathodes used in full cells were purchased from Canrd New Energy Technology Co., Ltd. The active material mass loadings for LFP and NCM811 were ~13 mg cm^{-2} and ~16 mg cm^{-2}, respectively. The galvanostatic cycling tests at different rates were conducted on the NEWARE battery testing system at 25 °C.

Electrochemical Characterization

The ion-conductivities of the QSSEs were measured using electrochemical impedance spectroscopy (EIS) with an amplitude of 10 mV of AC voltage over a frequency range of 0.1 Hz to 1 MHz. The electrolyte was sandwiched between two current collectors made of stainless steel (SS). And the electrolyte's ion-conductivity σ was calculated using the equation below.

$$\boldsymbol{\sigma = \frac{L}{SR}}$$

where $\boldsymbol{L}$, $\boldsymbol{S}$, and $\boldsymbol{R}$ denote the electrolyte thickness, contact area between electrode and electrolyte, and receptive resistance.

The chemical stability of the electrolytes was tested on Li||QSSE||SS cells with linear sweep voltammetry (LSV) at a scanning rate of 1 mV s^{-1}.

The lithium-ion transference number ($\boldsymbol{t_{Li^+}}$)of QSSEs was calculated from Bruce–Vincent–Evans equation

$$\boldsymbol{t_{Li^+} = \frac{I_S(\Delta V - I_0 R_0)}{I_0(\Delta V - I_S R_S)}}$$

where $\boldsymbol{\Delta V}$ is the applied polarization voltage (10 mV), $\boldsymbol{I_0}$ and $\boldsymbol{I_S}$ represent the initial and steady-state currents, and $\boldsymbol{R_0}$ and $\boldsymbol{R_S}$ are the initial and steady-state resistances which were derived from EIS measurements, respectively.

The activation energy of lithium-ion migration in the investigated electrolytes is calculated by Arrhenius equation:

$$\frac{1}{\sigma(T)} = A \cdot exp\left(\frac{-E_a}{k_b \cdot T}\right)$$

where $\boldsymbol{\sigma(T)}$ is the ionic conductivity at the absolute temperature $\boldsymbol{T}$, $\boldsymbol{A}$ is the pre-exponential factor, $\boldsymbol{E_a}$ is the apparent activation energy, and $\boldsymbol{k_b}$ stands for the Boltzmann constant, respectively.

Computational Details.

First-principles electronic structure calculations were carried out using density functional theory (DFT) as implemented in the Vienna Ab initio Simulation Package (VASP), and the results were visualized in VESTA. [3-6] The exchange-correlation

functional was approximated using the generalized gradient approximation proposed by Perdew, Burke, and Ernzerhof (GGA-PBE). [7] The cutoff for plane-wave energy was 600 eV. [8] In our DFT calculations, we use a 6 × 6 supercell of monolayer *h*-BN absorbed by Li^+ and an anion to simulate the interaction between Li^+ (as well as anions) and hexagonal boron nitride nanosheets (*h*-BN). To avoid adjacent interactions, a vacuum layer of 30 Å was introduced along the vertical direction. The Brillouin zone is sampled using Γ point. All structures were fully optimized until the energy and residual force were less than 10^{-5} eV and 0.02eV $Å^{-1}$, respectively.

The adsorption energy of Li^+ or an anion on monolayer *h*-BN was defined as $E_f = E_{total} - E_{sub} - E_{ion}$, where E_{sub} was the energy of the bared monolayer *h*-BN sheet, E_{total} was the energy of the corresponding system with cation or anion adsorbed, and E_{ion} was the energy of the lithium-ion or anion. Because lithium salt as a solute was dissolved in the vinylene carbonate solvent, the interaction between solvent molecules and ions should be taken into account in our DFT calculations. The energy of a single ion (E_{ion}) was calculated by a self-consistent implicit solvation model,[9, 10] which could well describe the dielectric screening of a solute embedded in an implicit solvent. The electrolyte model considering the solvent effect was implemented in the VASPsol code, which was used in our calculations to obtain the energy of the solute's ion[11]

We used AIMD calculations to simulate the evolution of lithium ions in a solvent filled with BNNFs and vinylene carbonate. AIMD simulations were run at a time step of 0.5 fs, and canonical ensemble (NVT) conditions were imposed by a Nose-Hoover thermostat set to 300 K. The GGA-PBE exchange-correlation functional was used with a plane-wave cutoff energy of 550 eV. For all of the MD trajectories, we let the entire system evolve for ~1 ps (2000 steps) to reach equilibrium. Following that, statistical sampling was carried out during the ~7 ps (14000 steps). Because of the size of the supercells, only Γ point was used to sample the Brillouin zone.

The periodic boundary condition was used in these models with and without the addition of h-BN. The volume for the h-BN model is (15.07 × 15.07 × 15.00) $Å^3$. Because the entire system should be charge neutral, each model included the Li^+, ClO_4^- ($BF_2C_2O_4^-$), and 28 vinylene carbonate molecules, with the density of vinylene

carbonate in the supercell remaining around 1.355 g/cm^3. The distance between neighboring h-BN sheets is large enough to prevent interactions between adjacent h-BN layers. Because the binding interaction between BNNFs and lithium-ion is stronger than that between anion and BNNFs in the electrolyte with BNNFs, we set that lithium-ion is adsorbed on the surface of the BN nanosheet in the initial configuration (the lithium-ion is initially about 2 Å away from the surface of the BN nanosheet). In the initial configuration (t = 0ps), we placed the Li^+ and ClO_4^- ($BF_2C_2O_4^-$) far apart, but close to the *h*-BN sheet on the same side. We reduce the vertical size of the supercell in the model without *h*-BN to ensure the density of vinylene carbonate molecules is similar to that in the model with h-BN. It has a volume of (15.07 × 15.07 × 11.80) Å^3, and in the initial setting (t = 0ps), we separated the Li^+ and ClO_4^- ($BF_2C_2O_4^-$). Furthermore, we looked at how the distance between Li^+ and the corresponding anion changed over time to see if it reflected the electrolyte system's damping of lithium-ion migration. The damping of lithium-ion migration became small when the distance between Li^+ and anion changed significantly, and vice versa.

The standard deviation (SD) is calculated by the formula as follows:

$$SD = \sqrt{\frac{1}{N}\sum_{i=1}^{N}(x_i - \mu)^2}$$

in which μ signifies the mean distance between $BF_2C_2O_4^-$ and lithium-ion in the time evolution of 7ps, x_i represents sampling data, that is, the distance value at each sampling point, N stands for the total number of sampling data.

Supplementary Figures

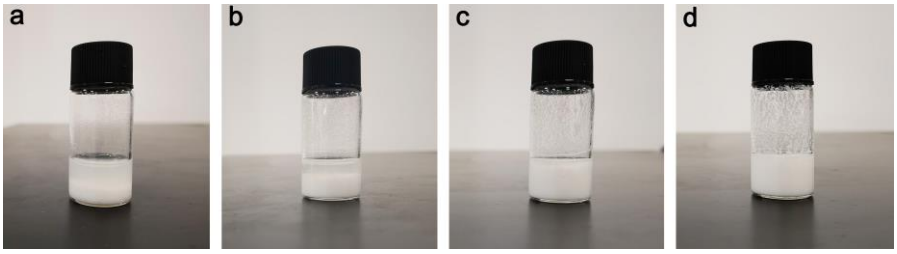

Figure S1. Digital images of BNNFs dispersed in VCA with different concentrations of a) 2.0 mg mL^{-1}, b) 4.0 mg mL^{-1}, c) 5.8 mg $mL^{-1,}$ and d) 6.1 mg mL^{-1}.

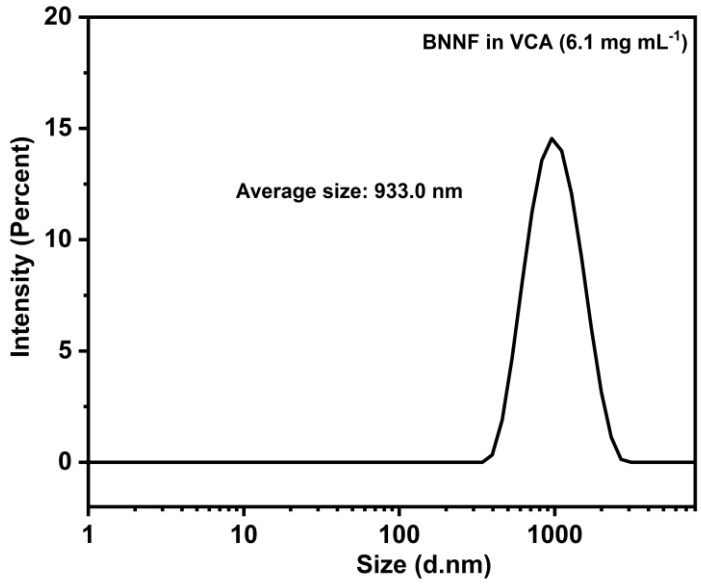

Figure S2. Particle size distribution of BNNFs in VCA (6.1 mg mL^{-1}).

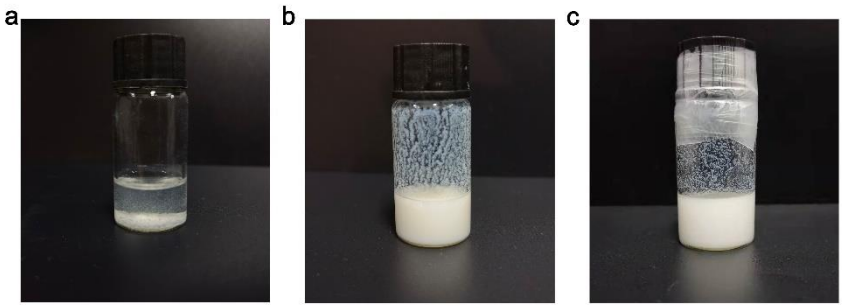

Figure S3. Digital photos of VCA-BNNF liquid dispersion a) before ultrasonic dispersion, b) after ultrasonic dispersion, and **c**) after 72 hours standing.

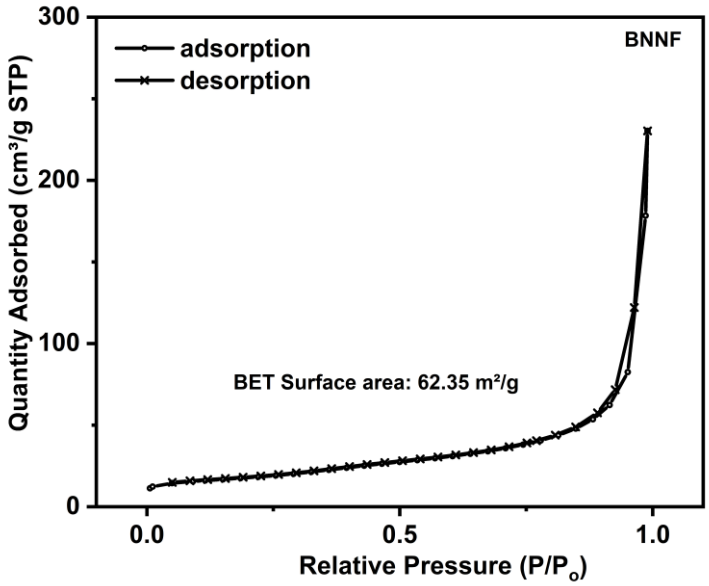

Figure S4. Isotherm linear plot of BNNFs.

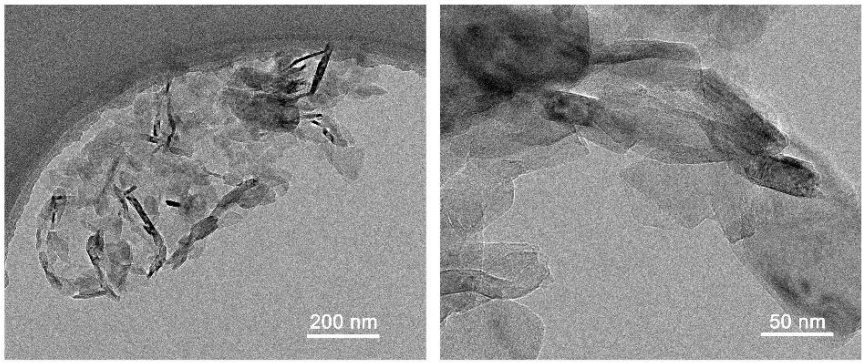

Figure S5. The TEM image of BNNFs with different magnifications.

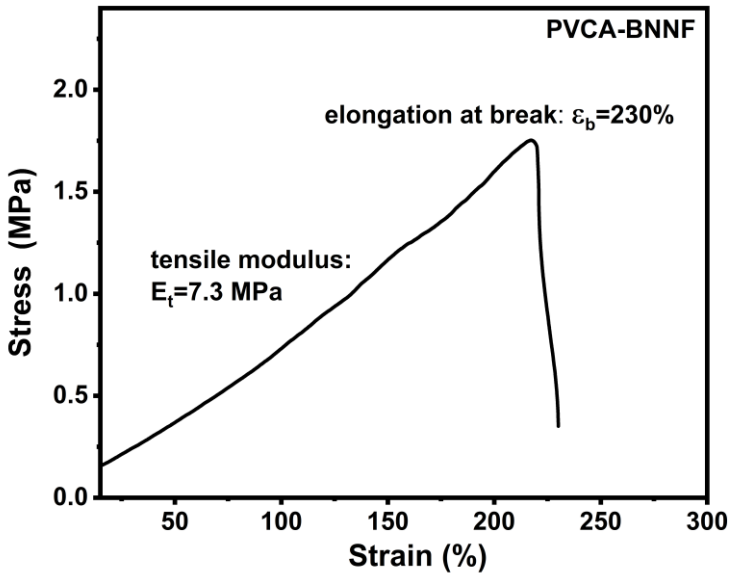

Figure S6. The result of tensile testing of PVCA-BNNF QSSE.

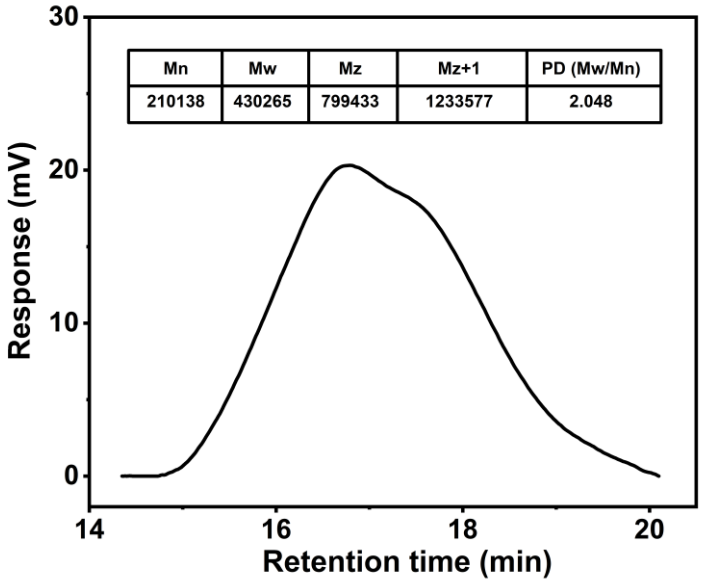

Figure S7. GPC results of PVCA-BNNF QSSE.

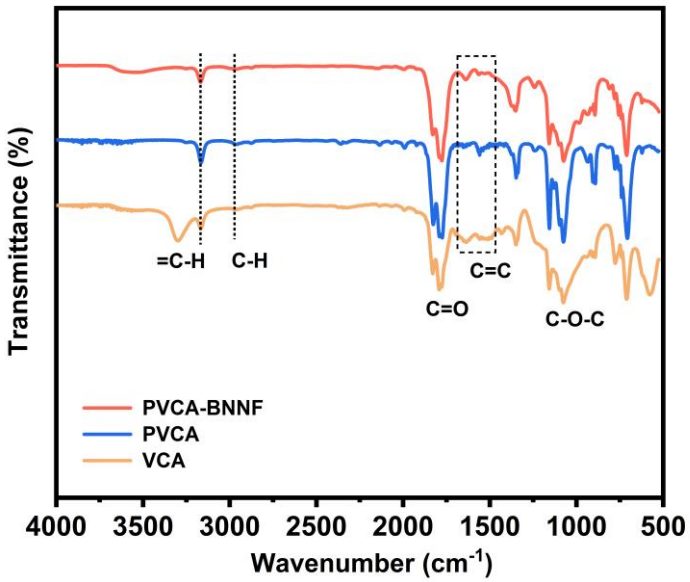

Figure S8. FT-IR spectra of VCA precursor, PVCA QSSE and PVCA-BNNF QSSE.

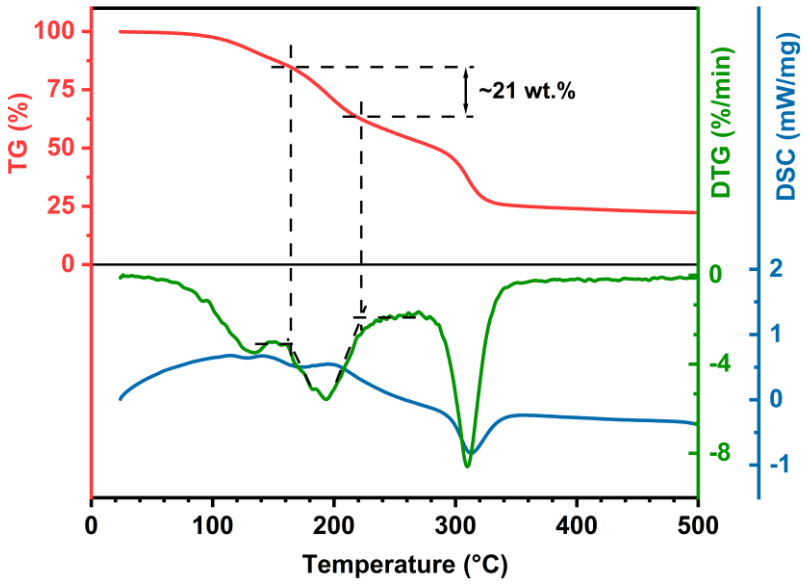

Figure S9. TG, DSC, and DTG curves of PVCA-BNNF QSSE from room temperature to 500 ℃.

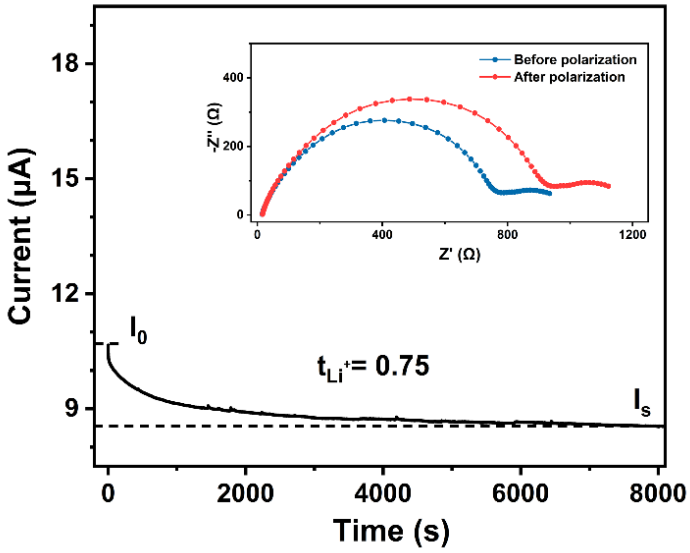

Figure S10. The current variation with time during polarization of a Li||PVCA-BNNF||Li symmetrical cell utilizing $LiClO_4$ at 25 °C, with a total applied potential difference of 10 mV. Inset shows the AC impedance spectra of symmetric cells.

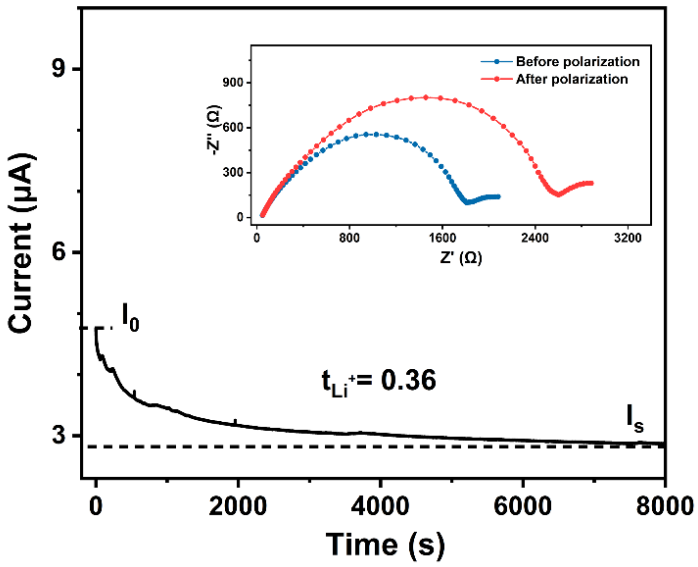

Figure S11. The current variation with time during polarization of a Li||PVCA||Li symmetrical cell utilizing LiDFOB at 25 °C, with a total applied potential difference of 10 mV. Inset shows the AC impedance spectra of symmetric cells.

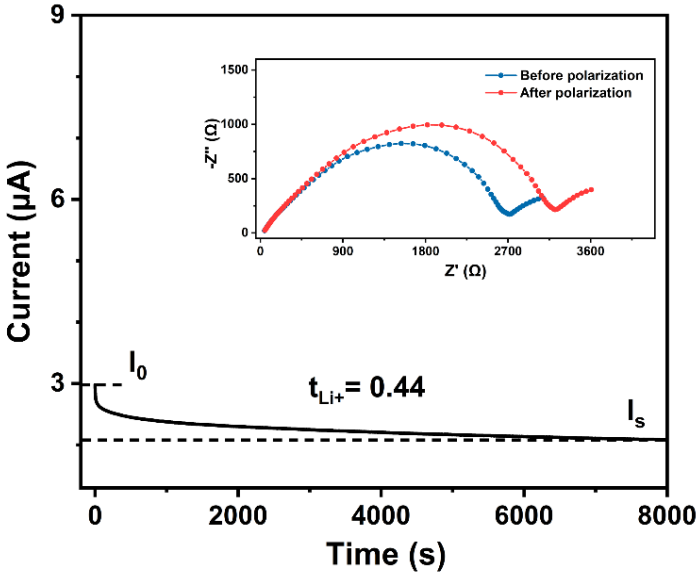

Figure S12. The current variation with time during polarization of a Li||PVCA||Li symmetrical cell utilizing $LiClO_4$ at 25 °C, with a total applied potential difference of 10 mV. Inset shows the AC impedance spectra of symmetric cells.

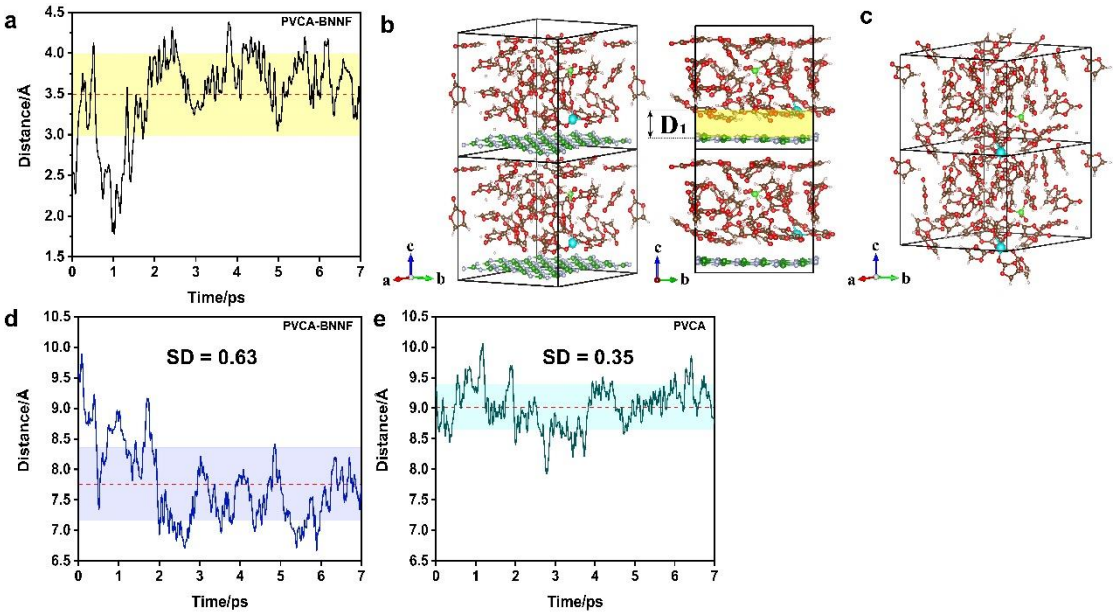

Figure S13. AIMD results of PVCA-BNNF QSSE utilizing $LiClO_4$. a) Change of vertical distance between lithium ion and BN surface under the simulated time scale, in which the red dotted line represents the average distance and shaded areas represent the range of positive and negative *SD* above and below the average distance. AIMD models b) with BNNF and c) without BNNF system. C, O, H, B, N, F, and Li atoms are shown as brown, red, pink, green, silver, gray, and blue balls, respectively, in which Vinylene carbonate solvent molecules fill the entire empty space and letter D_1 represents the vertical distance between lithium ion and BN surface shown in a). The distance between lithium ion and ClO_4^- varies with time in the system d) with BNNF and e) without BNNF, in which *SD* is the corresponding standard deviation and the red dotted line represents the average distance. The shaded areas represent the range of positive and negative σ above and below the average distance.

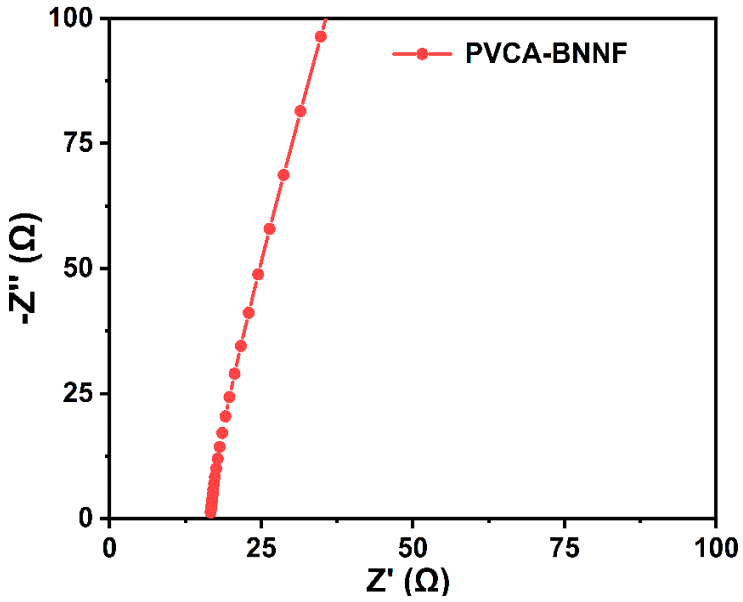

Figure S14. Nyquist plot of SS||PVCA-BNNF||SS cell at 20 °C.

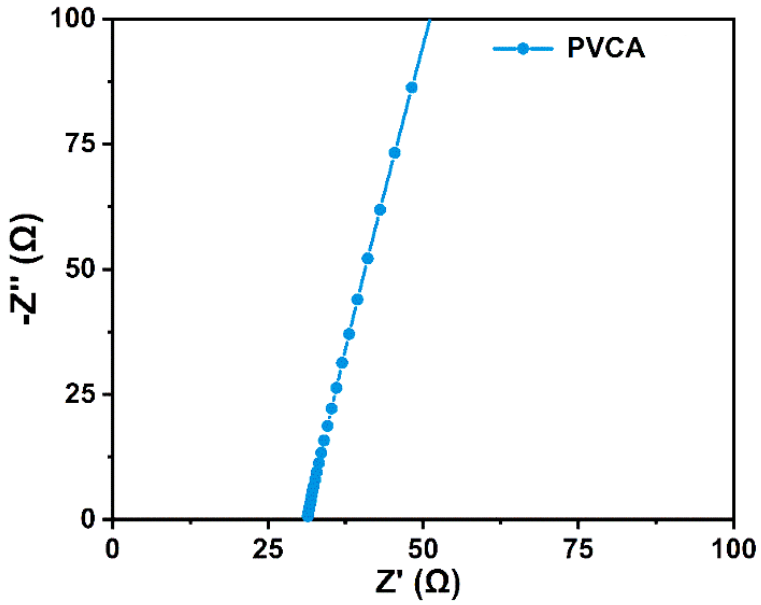

Figure S15. Nyquist plot of SS||PVCA||SS cell at 20 ℃.

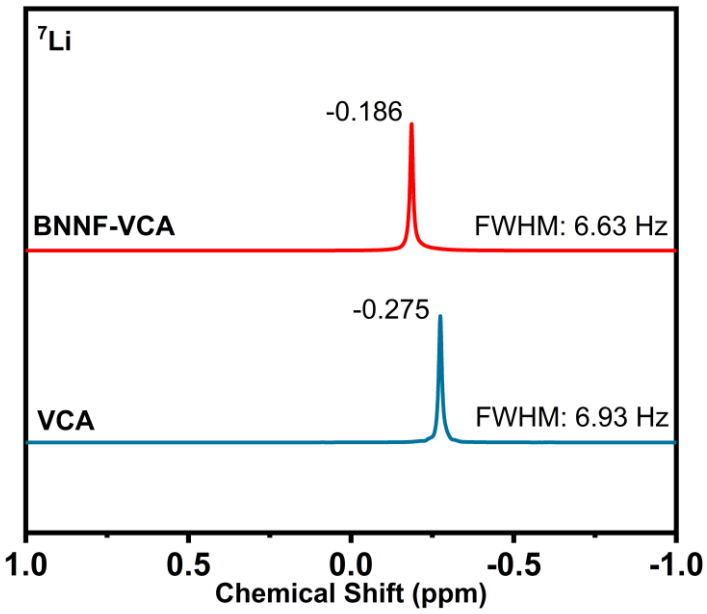

Figure S16. NMR spectra of VCA-BNNF and VCA (1M LiDFOB) with full width at half maximum (FWHM) of each sample.

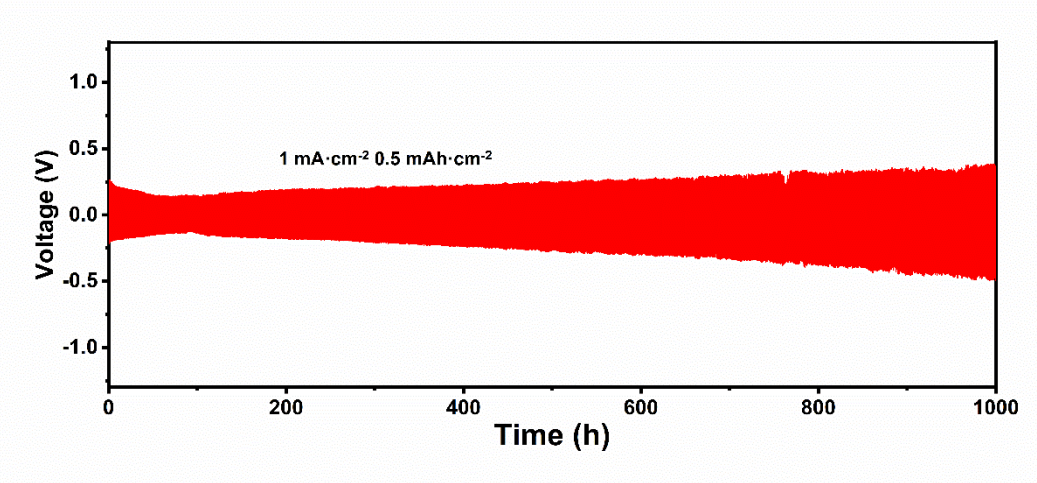

Figure S17. Galvanostatic cycling profiles of symmetric Li/Li cell with PVCA-BNNF QSSE at 1 mA cm^{-2} and 0.5 mAh cm^{-2}.

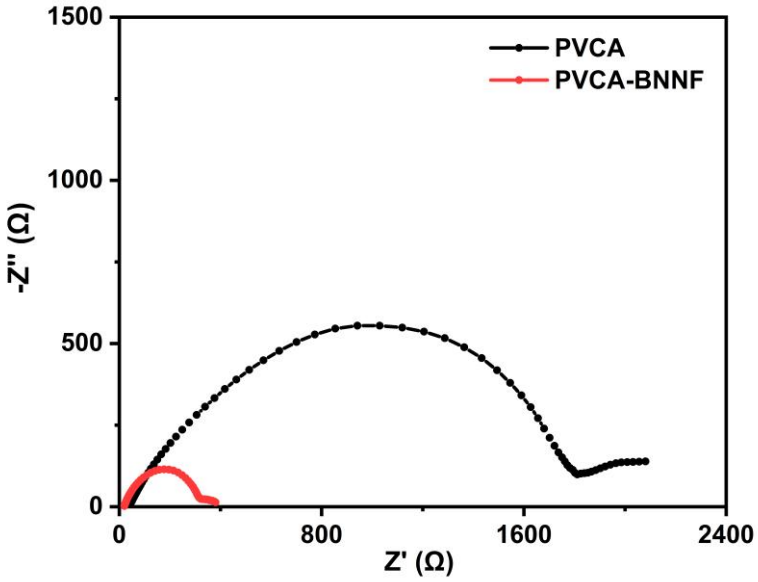

Figure S18. Nyquist plots of Li||PVCA||Li and Li||PVCA-BNNF||Li.

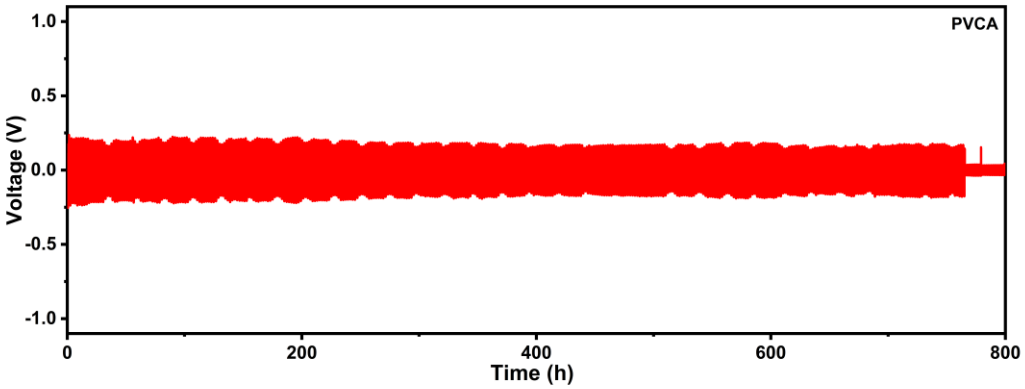

Figure S19. Galvanostatic cycling profiles of symmetric Li/Li cell with PVCA QSSE at 0.1 mA cm^{-2} and 0.1 mAh cm^{-2}.

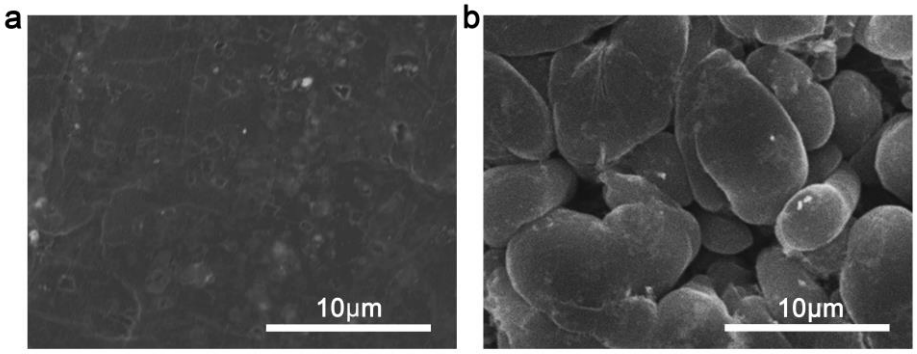

Figure S20. SEM image of the top view of the surface of Li anode in cells assembled with a) PVCA-BNNF and b) non-aqueous liquid electrolyte (1M $LiPF_6$ in EC/DEC/DMC) after 0.5 mAh cm^{-2} Li is deposited at 0.5 mA cm^{-2}.

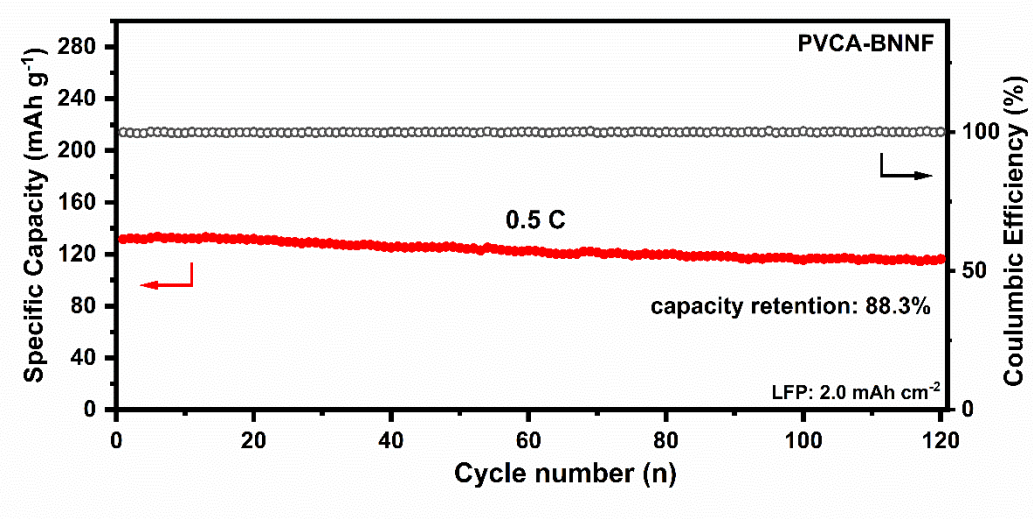

Figure S21. Cycling performance of Li/LFP cell with PVCA-BNNF QSSE at 0.5 C.

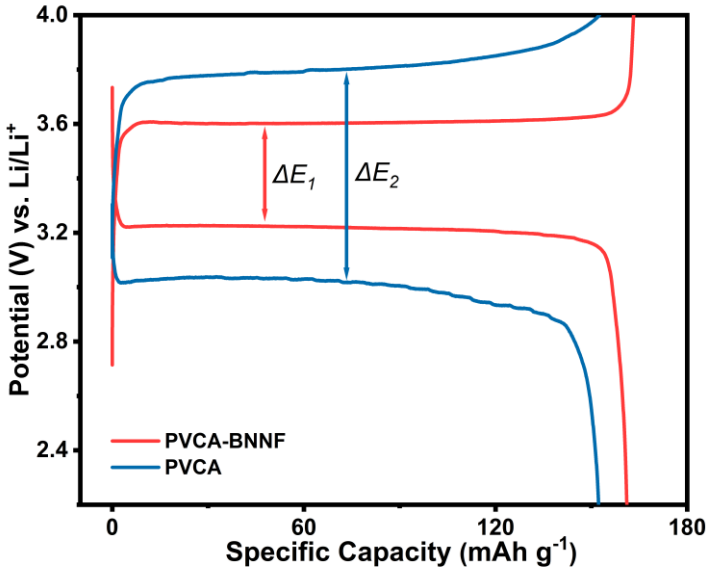

Figure S22. Charge/discharge profiles of LFP||PVCA-BNNF||Li and LFP||PVCA||Li.

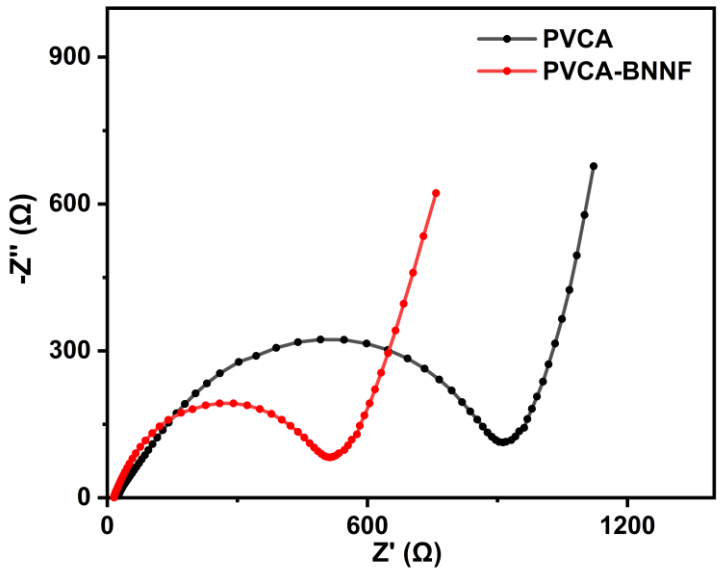

Figure S23. Nyquist plots of NCM||PVCA||Li and NCM||PVCA-BNNF||Li.

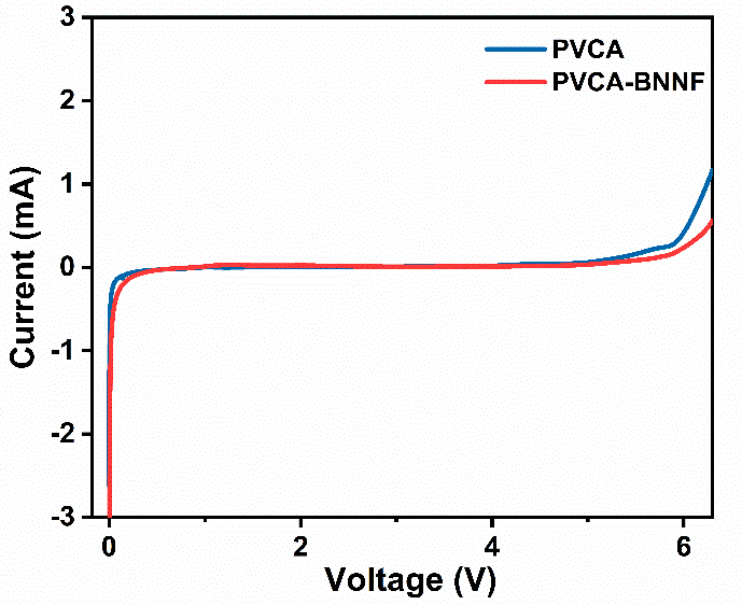

Figure S24. LSV curves of PVCA QSSE and PVCA-BNNF QSSE with a voltage window from 0V to 6.2V.

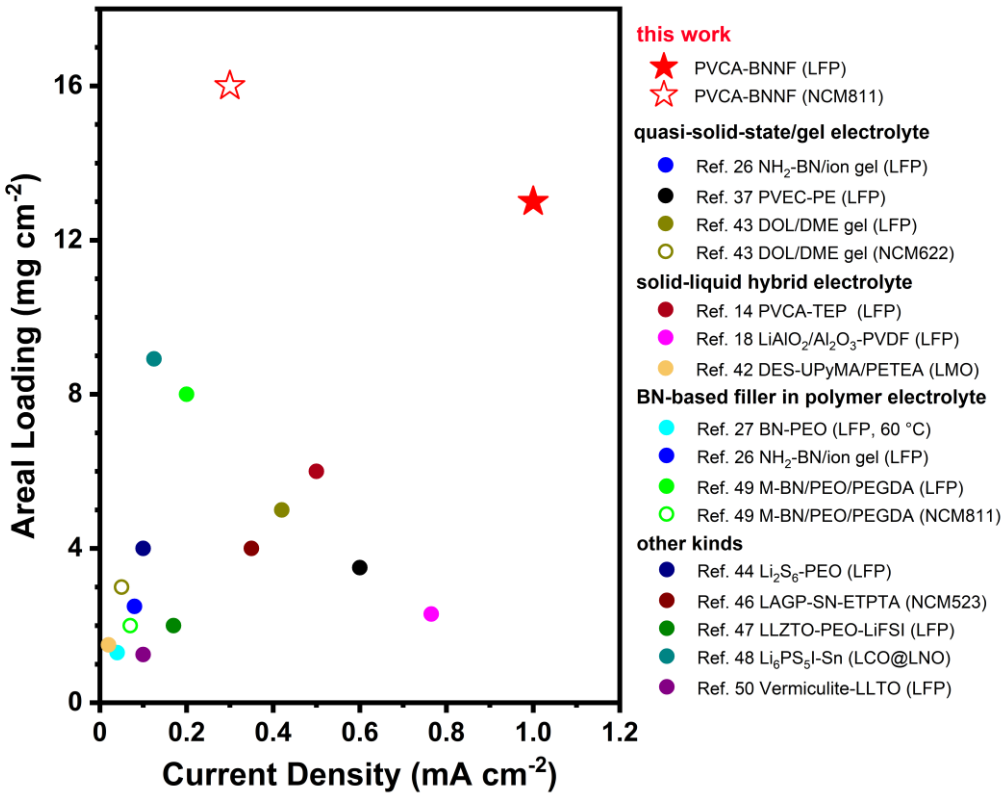

Figure S25. Comparison of the areal loading of the cathodes and current densities adopted in this work and other works previously reported.

Reference

(1) Hui, F.; Villena, M. A.; Fang, W.; Lu, A.-Y.; Kong, J.; Shi, Y.; Jing, X.; Zhu, K.; Lanza, M. Synthesis of large-area multilayer hexagonal boron nitride sheets on iron substrates and its use in resistive switching devices. *2D Mater.* **2018**, *5* (3), 031011-031017.

(2) Lee, J. S.; Choi, S. H.; Yun, S. J.; Kim, Y. I.; Boandoh, S.; Park, J.-H.; Shin, B. G.; Ko, H.; Lee, S. H.; Kim, Y.-M. Wafer-scale single-crystal hexagonal boron nitride film via self-collimated grain formation. *Science* **2018**, *362* (6416), 817-821.

(3) Momma, K.; Izumi, F. VESTA 3 for three-dimensional visualization of crystal, volumetric, and morphology data. *Journal of applied crystallography* **2011**, *44* (6), 1272-1276.

(4) Momma, K.; Izumi, F. VESTA: a three-dimensional visualization system for electronic and structural analysis. *Journal of Applied Crystallography* **2008**, *41* (3), 653-658.

(5) Kresse, G.; Hafner, J. Ab initio molecular dynamics for open-shell transition metals. *Physical Review B* **1993**, *48* (17), 13115.

(6) Kresse, G.; Furthmüller, J. Efficiency of ab-initio total energy calculations for metals and semiconductors using a plane-wave basis set. *Computational materials science* **1996**, *6* (1), 15-50.

(7) Perdew, J. P.; Burke, K.; Ernzerhof, M. Generalized gradient approximation made simple. *Physical review letters* **1996**, *77* (18), 3865.

(8) Kresse, G.; Joubert, D. From ultrasoft pseudopotentials to the projector augmented-wave method. *Physical review b* **1999**, *59* (3), 1758.

(9) Mathew, K.; Sundararaman, R.; Letchworth-Weaver, K.; Arias, T.; Hennig, R. G. Implicit solvation model for density-functional study of nanocrystal surfaces and reaction pathways. *The Journal of chemical physics* **2014**, *140* (8), 084106.

(10) Mathew, K.; Kolluru, V. C.; Mula, S.; Steinmann, S. N.; Hennig, R. G. Implicit self-consistent electrolyte model in plane-wave density-functional theory. *The Journal of Chemical Physics* **2019**, *151* (23), 234101.

(11) Kiran Mathew, D. R. H. Solvation model for the plane wave DFT code VASP. **2019**.